Proceedings of the 20th International Conference on Soil Mechanics and Geotechnical Engineering– Rahman and Jaksa (Eds)

Experimental evaluation of shear strength fluctuations of clayey soils due to multiple cyclic loads

Évaluation expérimentale des fluctuations de la résistance au cisaillement des sols argileux en raison de multiples charges cycliques

Beena Ajmera
Department of Civil, Construction and Environmental Engineering, Iowa State University, USA, bajmera@iastate.edu

Binod Tiwari
Office of Research and Sponsored Projects and Department of Civil and Environmental Engineering, California State University, Fullerton, USA, btiwari@fullerton.edu

Muhammad Shahid Iqbal & Tiffany Meeks
Department of Civil, Construction and Environmental Engineering, North Dakota State University, USA

ABSTRACT: Often seismic loading causes instability and/or failure of geotechnical structures such as foundations, slopes, and embankments in the form of settlements, landslides, and liquefaction. Numerous researchers who have worked on cyclic behavior and strength loss of clayey soils after earthquake loading have focused on the strength reductions immediately after a single cyclic event. Little work is found on the changes in the shear strength of clayey soils after multiple cyclic events representing the main shock and aftershocks in an earthquake sequence. To do so, cyclic direct simple shear tests were conducted on kaolinite specimens. The shear strengths of this soil were measured immediately after a sequence of cyclic loads. The results obtained were used to develop cyclic strength curves and evaluate the strength degradation in the clayey soils. The degree of consolidation between cyclic loads was found to impact the cyclic resistance available during the following cyclic load as well as the resulting strength degradation.

RÉSUMÉ : Souvent, les charges sismiques provoquent une instabilité et/ou une défaillance des structures géotechniques telles que les fondations, les pentes et les remblais sous forme de tassements, de glissements de terrain et de liquéfaction. De nombreux chercheurs qui ont travaillé sur le comportement cyclique et la perte de résistance des sols argileux après une charge sismique se sont concentrés sur les réductions de résistance immédiatement après un seul événement cyclique. Peu de travaux sont trouvés sur les changements de la résistance au cisaillement des sols argileux après de multiples événements cycliques représentant le choc principal et les répliques d'une séquence sismique. Pour ce faire, des essais cycliques de cisaillement direct simple ont été menés sur des échantillons de kaolinite. Les résistances au cisaillement de ce sol ont été mesurées immédiatement après une séquence de charges cycliques. Les résultats obtenus ont été utilisés pour développer des courbes de résistance cyclique et évaluer la dégradation de la résistance dans les sols argileux. Le degré de consolidation entre les charges cycliques s'est avéré avoir un impact sur la résistance cyclique disponible pendant la charge cyclique suivante ainsi que sur la dégradation de la résistance qui en résulte.

KEYWORDS: Shear strength degradation, dynamic loading, cyclic simple shear tests, fine-grained soils, multiple cyclic events

1 INTRODUCTION

Seismic loading can cause a partial or complete loss of strength in soils resulting in instabilities and/or failure of geotechnical structures. The strength degradations induced in fine-grained soils because of seismic loading are not well understood, despite their severe consequences. The Anchorage Landslide (or Fourth Avenue Slide) after the 1964 Alaska earthquake (Stark & Contreras 1998, Boulanger & Idriss 2004) and more recently, the Vine Road Embankment failure after the 2018 Alaska Earthquake (Franke et al. 2019) are two prime examples. Tiwari et al. (2018) provided a detailed study of landslide movements in a gently sloped ground near Lokanthali, Nepal after the 2015 Gorkha earthquake. Through their numerical modeling, they illustrated that the observed deformations were not induced solely by the ground shaking. Instead, these deformations were induced when the ground shaking was combined with the resulting strength degradations in the underlying kalimati (black cotton soil). As these examples illustrated, an understanding of the strength degradations induced by cyclic loading is necessary to properly design and evaluate the stability of geotechnical structures under such conditions.

The strength degradations induced by seismic loading in fine-grained soils have been shown to be influenced by a number of factors. These include the plasticity characteristics (Ishihara & Yasuda 1980, Tan & Vucetic 1989, Bahr 1991, Ishihara 1993, Hyodo et al. 1998, Matsui et al. 1999, Guo & Prakash 1999, Hyodo et al. 2000, Bray et al. 2004, Gratchev et al. 2006; Bray & Sancio 2006, Ajmera et al. 2019), clay mineralogy (Sandoval 1989, Prakash & Sandoval 1992, Gratchev et al. 2006, Beroya et al. 2009, Ajmera et al. 2019), and excess pore pressure at the end of cyclic loading (Yasuhara 1994, Thammathiwat & Chim-oye 2004, Ajmera et al. 2019). Ajmera et al. (2019) provides a comprehensive evaluation of the strength degradations in fine-grained soils examined through an extensive laboratory testing program. They established a unique relationship between the normalized undrained strength ratio (*Norm. USR*) and the post-cyclic effective stress ratio (*PC-ESR*). The normalized undrained strength ratio is defined as given in Equation 1, where s_u is the static undrained shear strength, $s_{u,pc}$ is the post-cyclic undrained shear strength (the undrained shear strength measured immediately after the termination of a cyclic load), σ'_c is the consolidation pressure before the application of any cyclic loads, and σ'_{pc} is the post-cyclic effective stress, or the effective stress immediately after the termination of a cyclic load. The post-cyclic effective stress ratio is computed using Equation 2.

$$Norm.USR = \frac{s_{u,pc}/\sigma'_{pc}}{s_u/\sigma'_c} \quad (1)$$

$$PC - ESR = \frac{\sigma'_c}{\sigma'_{pc}} \quad (2)$$

While the relationships presented by Ajmera et al. (2019) allow for the estimation of the undrained shear strengths of fine-grained soils after cyclic loading, the work focused on the strength degradations from a single cyclic loading event. In reality, fine-grained soils in seismic regions are subjected to multiple cyclic events in the form of the main shock from an earthquake followed by a series of aftershocks. This sequence of seismic events could exacerbate the strength degradations in fine-grained soils leading to subsequent failures or larger disasters. Thus, it is pertinent that methods to estimate the strength degradations in fine-grained soils subjected to multiple cyclic loading events be developed. This study builds on the work in Ajmera et al. (2019) by examining the strength degradations in instances when one aftershock with an equal or lower peak ground acceleration follows the main shock.

2 METHODOLOGY

2.1 *Soil tested*

Kaolinite, purchased from Ward's Natural Science, was used in this study for all of the testing conducted. The soil had a maximum particle size of 0.02 mm with a clay fraction (percentage of particles smaller than 2 μm) of 70%. It has a liquid limit and plasticity index of 73 and 28, respectively. Normally consolidated kaolinite has an undrained strength ratio of 0.30 (Ajmera et al. 2019).

2.2 *Sample preparation*

To prepare the dry powdered kaolinite for testing, it was mixed with de-aired distilled water. An initial moisture content equal to the liquid limit of 73% was used. The resulting slurry was then allowed to hydrate for a minimum of 24 hours in an airtight container before any testing was conducted. Cyclic simple shear tests were then conducted using portions of the batch prepared slurry.

2.3 *Test apparatus*

A fully-automated, computer controlled SGI-type cyclic simple shear apparatus, manufactured by GeoComp, Inc. was used. A micro-stepper motor is used to apply the vertical loads and a servo motor is used to apply the horizontal loads. Horizontal and vertical loads are measured using a 10 kN capacity load cells. LVDTs with 50 mm capacities resolved to 7.6×10^{-5} mm are used to measure horizontal and vertical displacements.

2.4 *Cyclic simple shear test procedures*

The hydrated slurried kaolinite is used to prepare the test specimens. This slurry is placed in a rubber membrane confined by a stack of 34 Teflon® coated aluminum rings. Each Teflon® ring is 0.91 mm thick. The specimens have a diameter of 63.5 mm with an initial height of 25.4 mm. Under the K_o conditions, the vertical stress is increased to 25 kPa and the specimen is allowed to consolidate. The real-time consolidation curve is monitored and upon completion of the primary consolidation, the stress is doubled until a final consolidation pressure of 100 kPa is achieved. When the primary consolidation is completed at this final consolidation pressure, the specimen is subjected to stress-controlled, constant volume undrained cyclic loading.

Cyclic loads are applied in the form of a sinusoidal wave with a period of 2 sec. In this study, *CSR* is defined as the amplitude of the sinusoidal wave to the consolidation pressure. Cyclic loading is applied until the specimen experiences 10% double amplitude shear strain or 500 cycles of loading at a CSR of 0.21. The failure criteria were adapted from the recommendations in ASTM D5311/D5311M, which outlines the procedures for conducting load-controlled cyclic triaxial tests. Following the application of the first cyclic load, as described above, excess pore pressures generated during the cyclic loading were allowed to dissipate to obtain specimens at different degrees of consolidation before a second cyclic load was applied.

Different specimens were tested to achieve 20%, 40%, 60%, 80% and 100% dissipation of the pore pressures generated during the first cyclic load. If 100% of the excess pore pressure generated during the first cyclic load was allowed to dissipate, the effective and total stress acting on the specimen would be equal to 100 kPa. Otherwise, the total stress was equal to 100 kPa, but the effective stress was less than 100 kPa. After the targeted excess pore pressure dissipation was achieved, the specimen was subjected to a second cyclic load. This cyclic load also had sinusoidal waveform with a period of 2 sec. Several tests were conducted using different samples. Each sample was subjected to different CSRs during the second cyclic load. These CSRs ranged from 0.10 and 0.21. The second cyclic load was also applied until the specimen experienced 10% double amplitude shear strain or 500 cycles of loading, in accordance with the recommendations in ASTM D5311/D5311M.

Immediately following the application of the second cyclic load, the undrained shear strength of the specimen was measured. This shear strength is referred to as the post-cyclic undrained shear strength. It was measured under undrained strain-controlled loading applied at a rate of 5% per hour, per the recommendations in ASTM D6528. The static shear phase of the test was terminated when the peak undrained shear strength was obtained or when the specimen experienced 25% shear strain. This termination criterion is also consistent with ASTM D6528. A total of 35 cyclic simple shear tests were conducted in this study.

3 RESULTS

3.1 *Typical response*

Figure 1 illustrates the typical stress and pore pressure response obtained during the load-controlled cyclic simple shear tests conducted in this study. The specimen was subjected to a first cyclic load with an amplitude defined by a *CSR* of 0.21. The application of the cyclic loads on a soil specimen will result in an increase in the pore pressure with a corresponding reduction in the effective normal stress. Included in Figure 1 are the back-calculated responses for the pore pressure and the measured effective vertical stress. For reference, a horizontal line representing the total vertical stress of 100 kPa is also shown in Figure 1.

The variation in the shear strain with the number of cycles of loading during the first cyclic load is shown in Figure 2. The results in Figure 2 correspond to the same sample from Figure 1. In all of the tests, 10% double amplitude shear strain was achieved in 5 to 20 cycles with an average of 9 cycles during the application of the first cyclic load. However, the number of cycles required to achieve 10% double amplitude shear strain were greater in the second cyclic load in most of the tests. The only instances when the number of cycles required to achieve 10% double amplitude were lower during the second cyclic load where when the amplitude of the second cyclic load was the same as the first cyclic load or if little excess pore pressure dissipation occurred between the two cyclic loads when the amplitude of the second cyclic load was slightly lower than the first.

Typical stress-strain hysteresis loops are shown in Figure 3. The results in Figure 3 correspond to the specimen with the same test conditions as that for Figures 1 and 2. In all of the specimens tested, the area enclosed by the stress-strain hysteresis loops obtained during the second cyclic load was smaller than that enclosed by the hysteresis loops for the first cyclic load.

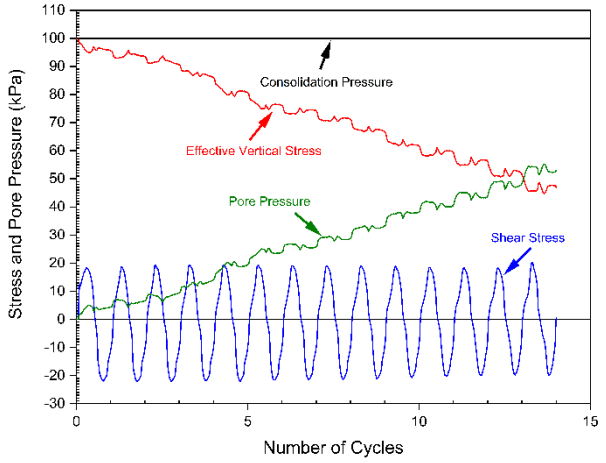

Figure 1. Typical stress and pore pressure response of kaolinite subjected cyclic loading with *CSR* is 0.21 for the first cyclic load.

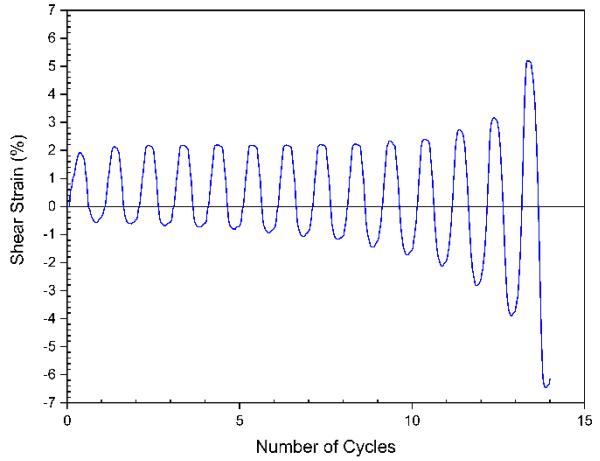

Figure 2. Typical variation in shear strain with number of cycles of loading for kaolinite. Results presented are for a kaolinite sample subjected to cyclic loading with *CSR* of 0.21 during the first cyclic load.

3.2 *Cyclic strength curves*

The cyclic resistance of soils during a seismic event can be quantified by cyclic strength curves. These curves delineate the number of cycles required to cause a specified level of double amplitude shear strain as a function of the *CSR*. Since all of the samples had similar values of *CSR* during the first cyclic load, cyclic strength curves from the first cyclic load are not discussed here. However, Ajmera et al. (2017) presented detailed analyses of the cyclic strength curves in fine-grained soils including the kaolinite tested in this study. The results in Ajmera et al. (2017) would indicate the cyclic resistance offered by kaolinite during the first cyclic load.

In this study, cyclic strength curves were developed based on the results obtained during the second cyclic load. Figure 4 presents the cyclic strength curves based on the number of cycles to cause 10% double amplitude shear strains. The number of cycles required to cause 10% double amplitude shear strain were interpolated to the nearest tenth of a cycle using the values of the double amplitude shear strain at the end of each cycle. The cyclic strength curves presented in Figure 4 correspond to the different degrees of consolidation between the two cyclic loads. As noted in Section 2.4, the degree of consolidation indicates the extent to which pore pressures generated during the first cyclic load were permitted to dissipate before the second cyclic load was applied. As Figure 4 demonstrates, as the excess pore pressures that developed during the first cyclic load were allowed to dissipate, the cyclic resistance offered by the sample during the second cyclic load increases.

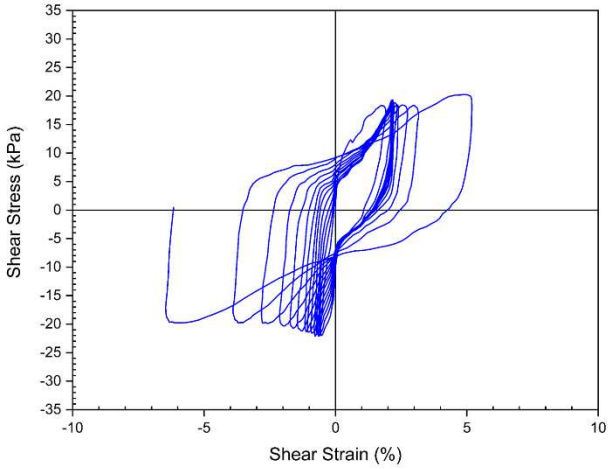

Figure 3. Typical stress-strain hysteresis loops for kaolinite subjected to cyclic loading with *CSR* equal to 0.21 for the first cyclic load.

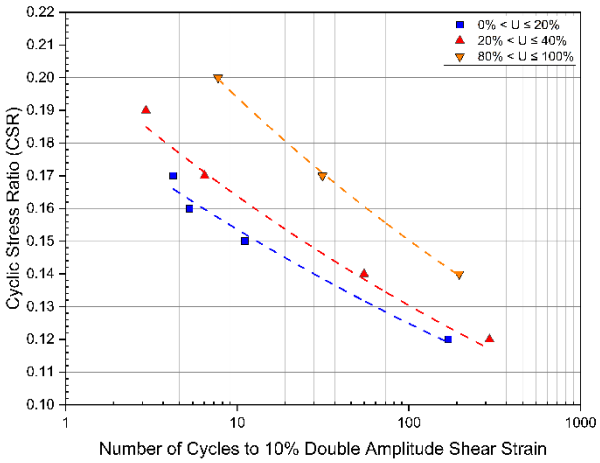

Figure 4. Representative cyclic strength curves for 10% double amplitude shear strain during the second cyclic load. *U* is the degree of consolidation.

Power functions can be used to represent cyclic strength curves (Ishihara et al. 1980, Ajmera et al. 2017). Specifically, the cyclic strength curve is expressed as shown in Equation 3, where a and b are curve fitting parameters and N_{10} is the number of cycles to 10% double amplitude shear strain. The curve fitting parameters and the coefficient of determination (R^2) for the best-fit power functions shown in Figure 4 are summarized in Table 1. As seen from Table 1, the value of a increases with an increase in the degree of consolidation between the cyclic loads, while the value of b remains nearly constant. This suggests that the cyclic strength curves will shift upward as pore pressures generated during the first cyclic load dissipate.

$$CSR = aN_{10}^{b} \tag{3}$$

3.3 *Degradation in undrained shear strength*

The degradation ratio (δ) is defined as the ratio of the post-cyclic undrained shear strength to the undrained shear strength of the sample without the application of cyclic loads, as shown in Equation 4. The variation of the degradation ratio with the degree of consolidation between cyclic loads is presented in Figure 5. This figure presents the degradation ratio computed immediately after the end of the second cyclic load relative the strength before any cyclic loads were applied. Figure 5 shows that as more excess pore pressures are allowed to dissipate between two cyclic loading events, the higher the degradation ratio. This implies that

the second cyclic load will cause a lower reduction in the undrained shear strength as more time elapses between two earthquake events.

$$\delta = \frac{s_{u,pc}}{s_u} \quad (2)$$

Table 1. Curve fitting parameters for cyclic strength curves.

Degree of Consolidation	*a*	*b*	R^2
$0 < U \leq 20\%$	0.189	-0.090	0.968
$20 < U \leq 40\%$	0.206	-0.099	0.952
$40 < U \leq 60\%$	0.221	-0.101	0.809
$60 < U \leq 80\%$	0.233	-0.100	0.902
$80 < U \leq 100\%$	0.250	-0.111	0.999

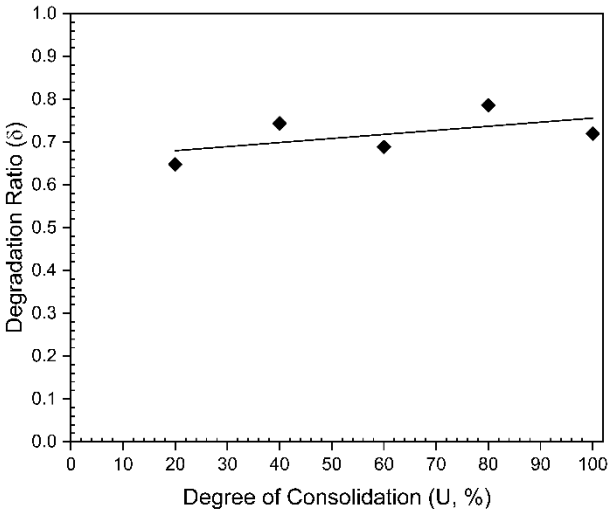

Figure 5. Variation in degradation ratio with the degree of consolidation between cyclic loads for tests. Data presented here correspond to those samples subjected to CSRs between 0.15 and 0.17 during the second cyclic load.

The results in Figure 5 correspond to the strength degradations when the second cyclic load at CSRs between 0.15 and 0.17. Detailed evaluation of the results at each of the CSRs tested indicated that the degradation ratio decreased as the CSR of the second cyclic load decreased at a constant degree of consolidation. In other words, the greater the severity of the second cyclic load in the sequence, the lower the post-cyclic undrained shear strength.

The relationship in Figure 5 is dependent on the cyclic stress ratio of the cyclic event and may depend on the soil type. However, the relationship proposed in Ajmera et al. (2019) between the normalized undrained strength and the post-cyclic effective stress ratios was found to eliminate the influence of clay mineralogy and the cyclic stress ratio. Building on this relationship, the normalized undrained strength ratio (Equation 1) and the post-cyclic effective stress ratio (Equation 2) were calculated for the specimens tested in this study. The resulting variation between these two parameters is shown in Figure 6. When preparing Figure 6, the post-cyclic effective vertical stress necessary to calculate the normalized undrained strength ratio and the post-cyclic effective stress ratio was taken as the value immediately after the end of the second cyclic load. It is equivalent to the effective vertical stress at the start of the static loading phase, during which the post-cyclic undrained shear strength will be measured. For comparison purposes, the relationship from Ajmera et al. (2019), shown in Equation 4, is also included in Figure 6.

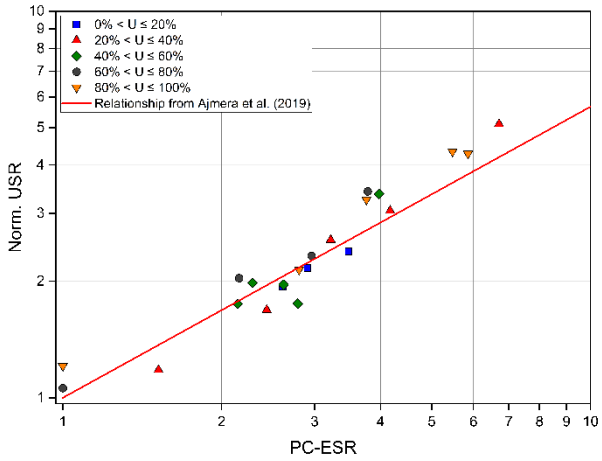

Figure 6. Variation in normalized undrained strength ratio as a function of post-cyclic effective stress ratio. Relationship proposed in Ajmera et al. (2019) for strengths immediately after one cyclic loading event is also included.

Although Equation 4 was developed to estimate the post-cyclic undrained shear strength in fine-grained soils immediately after one cyclic loading event, it appears to capture the behavior of fine-grained soils after multiple events. Specifically, as seen in Figure 6, the measured values of the normalized undrained strength ratio at the end of the second cyclic load are in close proximity to the relationship from Ajmera et al. (2019). Furthermore, the data in this study was measured after different amounts of excess pore pressure were allowed to dissipate. Therefore, the relationship proposed by Ajmera et al. (2019) is able to incorporate the effects of pore pressure dissipation between cyclic events.

$$Norm.USR = (PC - ESR)^{0.753} \quad (4)$$

3.4 *Comparison of measured and estimated normalized undrained strength ratios*

Using the post-cyclic effective stress ratios obtained during the cyclic simple shear tests conducted in this study, the normalized undrained strength ratio was estimated using Equation 4. A comparison of these estimated normalized strength ratios with the values measured during the cyclic simple shear testing is presented in Figure 7. Also included in Figure 7 are two lines representing a 15% deviation of the estimated normalized undrained strength ratios from those measured. Examining the figure, it is apparent that the nearly all of the estimates were within 15% of the measured values with only 5 data points having estimates slightly outside of this range.

Asides from providing the relationship for the best-fit power function (Equation 2), Ajmera et al. (2019) also presented curves indicating a ±95% prediction interval. The prediction interval describes the potential range within which 95% of the predictions from Equation 4 should lie. In Figure 7, open symbols are used to denote those estimates of the normalized undrained strength ratio that fell outside of the ±95% prediction interval. Only 7 of the predictions were outside of the prediction interval described by Ajmera et al. (2019).

Figure 7 clearly demonstrates that the relationship proposed in Ajmera et al. (2019) can appropriately estimate the normalized undrained strength ratios for the tests conducted in this study. This illustrates that the proposed relationship is suitable to estimate the post-cyclic undrained shear strengths after multiple cyclic events. It is further able to capture the impact of the dissipation of excess pore pressure on the post-cyclic undrained shear strengths.

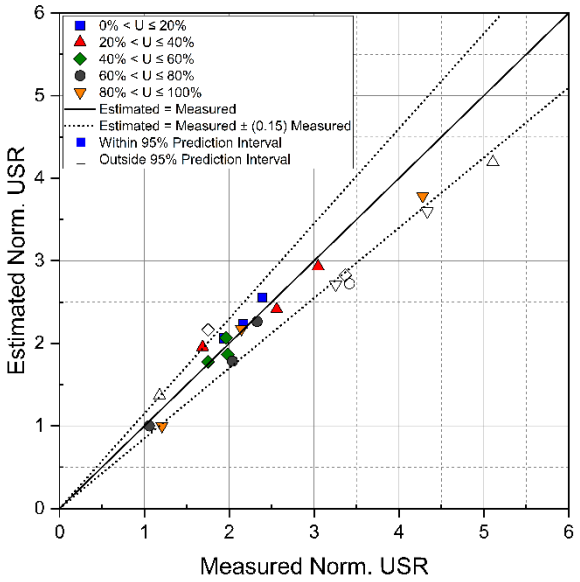

Figure 7. Comparison of normalized undrained strength ratios estimated using Equation 4 (Ajmera et al. 2019) with the measured normalized undrained strength ratios.

4 CONCLUSIONS

In this study, 35 cyclic simple shear tests were conducted on commercially available kaolinite. The specimens were subjected to multiple cyclic loading events during which the cyclic resistance was evaluated and following which the post-cyclic undrained shear strength was measured. The number of cycles required to cause 10% double amplitude shear strain were greater during the second cyclic load in the majority of the tests conducted. However, there was a decrease in the number of cycles required to cause 10% double amplitude shear strain when the amplitude of the second cyclic load was the same as that from the first cyclic load. The number of cycles would also be lower if the amplitude of the second cyclic load was slightly lower than the first cyclic load and little of excess pore pressure generated during the first cyclic load was allowed to dissipate.

Evaluation of the cyclic strength curves indicated that an increase in the degree of consolidation between the applications of the cyclic loads would result in an increase in the cyclic resistance. In particular, the cyclic strength curves were found to have similar slopes regardless of the amount of excess pore pressure allowed to dissipate. However, the vertical position of the cyclic strength curves would shift based on the degree of consolidation between cyclic loads.

Degradation ratios relating the post-cyclic undrained shear strength after the second cyclic load to the strength of the soil under static conditions were also evaluated. The results indicated that the post-cyclic undrained shear strength after the second cyclic load would be lower than the strength after the first cyclic load when the degree of consolidation between cyclic loads was less than 80%. However, an increase in the degree of consolidation between the cyclic loads would cause an increase in the degradation ratio. This suggests that the less severe degradations in the undrained shear strength could be expected as pore pressures generated after the first cyclic load dissipated.

The relationship proposed by Ajmera et al. (2019) between the normalized undrained strength ratio and the post-cyclic effective stress ratio was found to accurately predict the post-cyclic undrained shear strengths in kaolinite after multiple cyclic events and different degrees of excess pore pressure dissipation between these events. The equation proposed by Ajmera et al. (2019) can be used to provide an initial estimate of the post-cyclic undrained shear strengths.

Finally, it is noted that this paper is limited by the fact that it only contains the results from kaolinite samples subjected to a main shock (first cyclic load) followed a single aftershock (second cyclic load) with an equal or lower amplitude. Future work of the authors will include testing on fine-grained soils with different mineralogical compositions. In addition, the authors plan to perform tests in which the samples are subjected to multiple cyclic loads.

5 ACKNOWLEDGEMENTS

The authors would like to acknowledge the financial support from the North Dakota EPSCoR STEM grants program and the National Science Foundation (Award #1953102) to conduct this research.

6 REFERENCES

Ajmera B., Brandon T. and Tiwari B. 2017. Influence of index properties of cyclic strength curve for clay-silt mixtures. *Soil Dynamics and Earthquake Engineering* 102, 46-55.

Ajmera B., Brandon T. and Tiwari B. 2019. Characterization of the Reduction in Undrained Shear Strength in Fine-Grained Soils due to Cyclic Loading. *Journal of Geotechnical and Geoenvironmental Engineering* 145 (5), 04019017 1-10.

ASTM D5311/D5311M. 2013. Standard test method for load controlled cyclic triaxial strength of soil. American Society of Testing and Materials.

ASTM D6528. 2007. Standard test method for consolidated undrained simple shear testing of cohesive soils. American Society of Testing and Materials.

Bahr M.A. 1991. Mechanical behavior and modeling of saturated clays subjected to cyclic loading. Ph.D. Thesis, Osaka University.

Beroya M.A.A., Aydin A. and Katzenbach R. 2009. Insight into the effects of clay mineralogy on the cyclic behavior of silt-clay mixtures. *Engineering Geology* 106 (3-4), 154-162.

Boulanger R.W. and Idriss I.M. 2004. Evaluating the potential for liquefaction or cyclic failure of silts and clays. Report No. UCD/CGM-04/01. University of California, Davis.

Bray J.D. and Sancio R.B. 2006. Assessment of the liquefaction susceptibility of fine-grained soils. *Journal of Geotechnical and Geoenvironmental Engineering* 132 (9), 1165-1177.

Bray J.D., Sancio R.B., Riemer M. and Turan Durgunoghr H. 2004. Liquefaction susceptibility of fine-grained soils. *Proceedings of the 11th International Conference on Soil Dynamics and Earthquake Engineering and 3rd International Conference on Earthquake Geotechnical Engineering* 655-662.

Franke K.W., Koehler R., Atalay F., Beyzaei C.Z., Cabas A., Christie S., Dickenson S., Hastings N., Pierce I., Stuedlein A., Wang X., Yang Z. and ZhiQiang C. 2019. Geotechnical Engineering Reconnaissance of the 30 November 2018 Mw 7.1 Anchorage, Alaska Earthquake. GEER Report.

Gratchev I.B., Sassa K., Osipov V.I. and Sokolv V.N. 2006. The liquefaction of clayey soils under cyclic loading. *Engineering Geology* 86 (1), 70-84.

Guo T. and Prakash S. 1999. Liquefaction of silts and silt-clay mixtures. *Journal of Geotechnical and Geoenvironmental Engineering* 125 (8), 706-710.

Hyodo M., Ito S., Yamamoto Y. and Fujii T. 2000. Cyclic shear behavior of marine clays. *Proceedings of the 10th International Offshore and Polar Engineering Conference* 606-611.

Hyodo M., Yamamoto Y. and Fujii T. 1998. Cyclic shear failure and strength of undisturbed marine clays. *Proceedings of the 8th International Offshore and Polar Engineering Conference* 557-563.

Ishihara K. 1993. Liquefaction and flow failure during earthquakes. *Géotechnique* 43 (3), 351-415.

Ishihara K. and Yasuda S. 1980. Cyclic strengths of undisturbed cohesive soils of Western Tokyo. *Proceedings of the International Symposium on Soils under Cyclic and Transient Loading* 57-66.

Ishihara, K., Troncoso, J., Kawase, Y., and Takahashi, Y. 1980. Cyclic strength characteristics of tailings materials. *Soils and Foundations* 20 (4), 127-142.

Matsui T., Nabeshima Y. and El Mesmarym M.A. 1999. Degradation in cyclic shear behavior and soil properties of saturated clays. *Proceedings of the 9th International Offshore and Polar Engineering Conference* 536-541.

Prakash S. and Sandoval J.A. 1992. Liquefaction of low plasticity silts. *Soil Dynamics and Earthquake Engineering* 11 (7), 373-379.
Sandoval J.A. 1989. Liquefaction and settlement characteristics of silt soils. Ph.D. Thesis, University of Missouri-Rolla.
Stark T.D. and Contreras I.A. 1998. Fourth avenue landslide during 1964 Alaksan earthquake. *Journal of Geotechnical and Geoenvrionmental Engineering* 124 (2), 99-109.
Tan K. and Vucetic M. 1989. Behavior of medium and low plasticity clays under cyclic simple shear conditions. *Proceedings of the 4th International Conference on Soil Dynamics Engineering* 401-409.
Thammathiwat A. and Chim-Oye W. 2004. Behavior of strength and pore pressure of soft Bangkok clay under cyclic loading. *Thammasat International Journal of Science and Technology* 9 (4), 21-28.
Tiwari B., Pradel D., Ajmera B., Yamashiro B. and Khadka D. 2018. Landslide Movement at Lokanthali during the 2015 Earthquake in Gorkha, Nepal. *Journal of Geotechnical and Geoenvironmental Engineering* 144 (3), 05018001 1-12.
Yasuhara K. 1994. Postcyclic undrained strength of cohesive soils. *Journal of Geotechnical Engineering* 120 (11), 1961-1979.